THE JOURNAL OF PHYSICAL CHEMISTRY C

Article

Cite This: J. Phys. Chem. C 2018, 122, 18365−18375

pubs.acs.org/JPCC

Roles of Long-Range Hopping, Quantum Nuclear Effect, and Exciton Delocalization in Exciton Transport in Organic Semiconductors: A Multiscale Study

Yuqian Jiang,*[,†] Zhigang Shuai,*[,‡] and Minghua Liu[†]

[†]Laboratory for Nanosystem and Hierarchy Fabrication, CAS Center for Excellence in Nanoscience, National Center for Nanoscience and Technology, Beijing 100084, People's Republic of China

[‡]MOE Key Laboratory of Organic OptoElectronics and Molecular Engineering, Department of Chemistry, Tsinghua University, Beijing 100084, People's Republic of China

Supporting Information

ABSTRACT: Excitation energy transport in organic materials is of significance for determining the efficiency of light-harvesting systems. With the improved material preparation and device fabrication, the experimentally measured exciton diffusion length has increased rapidly in recent years and far exceeds the typical values found in synthetic organic systems on the order of 10 nm, calling for better understanding and evaluation of the intrinsic exciton diffusion property. We investigate the energy transport at three different levels, ranging from the semiclassical Marcus theory, to the quantum nuclear tunneling-mediated hopping, and eventually to the time-dependent exciton diffusion in organic semiconductors. All the calculations are based on first-principles evaluated molecular parameters. We find that the nuclear quantum effect can strongly enhance the exciton diffusion length by orders of magnitude. Both long-range energy transfer and exciton delocalization effects can also be identified.

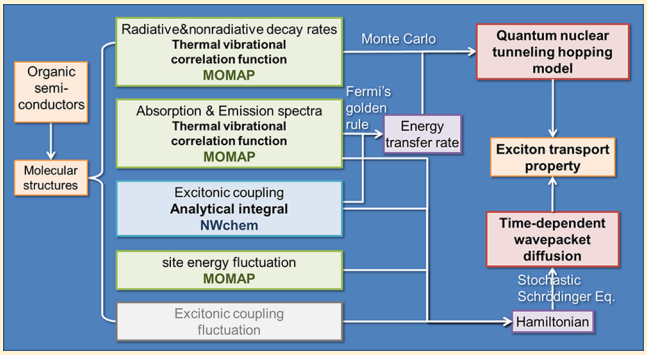

1. INTRODUCTION

Organic semiconductors (OSCs) have been widely applied to fabricate optoelectronic devices because of their unique photophysical characteristics as well as the easy-to-prepare and low-cost properties. As an indispensable electronic process in photophysics, the excitation energy transfer (EET) process plays a significant role in optoelectronic performances, especially for light-harvesting devices and photovoltaics.[1−4] The long-distance energy transport property can ensure relatively high light-harvesting efficiency in macroscopic systems. However, the singlet exciton diffusion length (L_D), which is related to the intermolecular excitonic coupling, molecular absorption and emission spectral overlap, the exciton lifetime, as well as structural defects, is typically of the order of only 10 nm in most of the OSCs.[5,6] In order to enhance the exciton transport ability, highly ordered organic materials with strengthened intermolecular interactions and reduced structural defects have been synthesized, and corresponding diffusion lengths can reach 100 nm and even micrometer magnitude. For example, L_D in the b direction for anthracene single crystals was shown to be 100 nm.[7] Particularly, Haedler et al. reported that the one-dimensional (1D) singlet exciton diffusion length in a single supramolecular nanofiber could reach 4 μm.[8] These results attract a growing number of attention in order to fabricate organic molecular materials with controllable energy transport properties for improving the optoelectronic performance. Thus, providing a comprehensive theoretical tool for predicting the exciton diffusion length in organic materials becomes significant.

For most OSCs with weak intermolecular excitonic couplings and strong intramolecular vibronic couplings, the incoherent hopping regime is considered to dominate the energy transport behavior. Hereinto, the Fürster resonance energy transfer rate[9,10] has gained tremendous popularity because of both the conceptual clarity and simplicity. The exciton diffusion length can be calculated by utilizing the experimental absorption and emission spectra, the fluorescence yield, and the exciton lifetime. Very often, such a calculated value could be underestimated because of the structural defects and boundary effects in real systems. Furthermore, neglecting the ab initio calculations on the molecular parameters makes the Fürster theory lack predictability. In fact, the Fürster transfer rate is derived from Fermi's golden rule (FGR), which has been directly applied to calculate the EET rate in organic systems by combining quantum chemistry calculations.[11,12] On the basis of the FGR rate, the kinetic Monte Carlo (KMC) method is usually used to simulate the random walking process

Received: July 19, 2018
Published: July 24, 2018

DOI: 10.1021/acs.jpcc.8b06918
J. Phys. Chem. C 2018, 122, 18365−18375

of exciton, and the exciton diffusion coefficient and length in organic materials can be finally obtained.[13,14] However, the approximate nature in the FGR theory, such as the displaced harmonic oscillator model,[14] the effective vibration mode,[12] or the sum-over-state method with limited normal modes and vibrational quanta,[15] could lead to a bias in the estimation of the nuclear tunneling effect, which has been found to play an important role in the EET process of organic systems,[12] like the situation in a carrier transport.[16,17] In addition, using the experimental exciton lifetime in calculating the exciton diffusion length makes the results empirical. Thus, to better understand the intrinsic transport mechanism in organic materials at the first-principles level, a parameter-free hopping model with a full nuclear quantum effect should be proposed.

As for the recently discovered long-distance energy transport materials with an indication of a transport behavior beyond the incoherent regime, the fully localized picture described by the Marcus theory or even FGR may not be applicable anymore. For instance, Haedler et al. used a simplified coherent transport model to confirm the supposition that it is the coherent transport regime dominating in the energy transport in the supramolecular nanofiber with 4 μm L_D. Sung et al. even directly observed delocalized excitons moving coherently along the chain of helical self-assembled perylene bisimides by ultrafast transient fluorescence spectroscopy.[18] For better understanding the exciton dynamics in systems with long diffusion lengths, mixed quantum/classical dynamics (MQCD) and full quantum dynamics (FQD) methods have been proposed to investigate energy transport. MQCD methods are more efficient but treat nuclear motions by classical dynamics, as represented by the tight-binding Hamiltonian theory based on the Haken−Strobl−Reineker model[19−21] and the dynamic disorder-limited transport theory based on the Su−Schrieffer−Heeger type model.[22] In contrast, FQD approaches can consider the nuclear quantum effect, such as the non-Markovian stochastic Schrüdinger equation[23,24] and nonperturbative hierarchically coupled equations of motion.[25] However, most of them are limited to the systems with only tens of sites because of the numerical convergence problem and computer memory limitation. Thus, FQD methods are rarely applied in studying real OSC systems. Zhong and Zhao have recently developed an efficient FQD method based on the stochastic Schrüdinger equation, namely, the time-dependent wave packet diffusion (TDWPD) approach,[23] which can deal with hundreds or even thousands of sites efficiently while considering the nuclear quantum effect through the harmonic oscillator model. The TDWPD method has shown good agreement with the path integral method and nonperturbative hierarchically coupled equations of motion in describing charge transport for small-sized symmetric systems. We have successfully applied the TDWPD method in interpreting the charge transport in a series of OSCs with high charge-carrier mobility and demonstrated the importance of the quantum nuclear effect and electronic delocalization in charge transport.[16]

Considering the excitation energy transport in real organic materials should fall in the range from incoherent to coherent regimes, we put forward a comprehensive tool to assess the intrinsic exciton diffusion property in OSCs. In the incoherent limit, we provide a quantum hopping model combining FGR with KMC simulation. Through utilizing the thermal vibration correlation function (TVCF) method for absorption and emission spectra as well as radiative and nonradiative decay rates that we developed earlier,[26,27] a parameter-free hopping model including the full quantum nuclear effect is put forward. Furthermore, a semiclassical hopping model based on the Marcus theory is provided for a comparison study. In the coherent regime, beyond one- or two-dimensional (2D) exciton dynamics typically performed by quantum mechanics because of the limit of computation cost,[19−22] we extend the TDWPD method to study the three-dimensional (3D) exciton diffusion property by considering the nuclear quantum effect and the exciton delocalization simultaneously. Then, we apply the three models to systematically study two typical OSCs, anthracene, and a difluoroboron β-diketonate derivative—BF_2bcz. Anthracene has long been focused on both experimental and theoretical research studies, and a wealth of data collected through experiment and theory are available to be compared with. Thus, we treat anthracene[28] as the benchmark system to validate the quantum hopping model and the TDPWD method. In addition, we take anthracene as an example to discuss in detail the impact of long-range energy transfer between nonadjacent dimers on exciton diffusion, which have been long neglected in previous investigations. As for BF_2bcz, Yang et al. have synthesized the first highly efficient artificial light-harvesting system based on its nanocrystal, which could funnel the excitation energy collected by a thousand chromophores to a single acceptor.[29] The exciton diffusion length can be roughly estimated by the relation $L_D \approx N^{D/A}\Phi_{EET}R_{D-D}/2Z$,[30] where $N^{D/A}$ is the molar ratio between donor and acceptor molecules, Φ_{EET} is the EET efficiency, R_{D-D} is the average intermolecular distance in the system, and Z is the space dimension (=3). According to the fluorescence spectra in different doping concentrations of acceptors as presented in ref 18 for different $N^{D/A}$ and Φ_{EET}, the exciton diffusion length can be estimated as ca. 700−800 nm. At a much larger concentration, it is reduced to only ∼100 nm because of the boundary effect, energy traps, and so forth. Thus, we believe that the intrinsic 3D exciton diffusion length in the BF_2bcz system should be larger than 100 nm. We also provide a thorough investigation on predicting the ultralong exciton diffusion length in the BF2bcz crystal and try to understand its mechanism by discussing the effects of the quantum nuclear vibration and exciton delocalization on its energy transport property.

2. FORMALISM AND COMPUTATIONAL APPROACH

2.1. Energy Transfer via Hopping.

$$D^* + A \rightarrow D + A^* \quad (1)$$

The rate of resonance energy transfer from the excited state of an energy-donating molecule (D*) to the ground state of an energy-accepting molecule (A) can be expressed as

$$k_{eet} = \frac{2\pi}{\hbar}|J_{DA}|^2 \int_0^{+\infty} d\omega \sigma_{emi}(\omega, T)\sigma_{abs}(\omega, T) \quad (2)$$

where J_{DA} is the intermolecular excitonic coupling, whereas $\sigma_{emi}(\omega,T)$ and $\sigma_{abs}(\omega,T)$ are the Franck−Condon integrals of donor emission and acceptor absorption spectra, respectively. Both of them can be expressed by the TVCF formalism.[31] Under the short-time approximation and the high-temperature limit, eq 2 can be simplified to the semiclassical regime, namely, Marcus theory

DOI: 10.1021/acs.jpcc.8b06918
J. Phys. Chem. C 2018, 122, 18365−18375

$$k_{eet} = \frac{1}{\hbar}|J_{DA}|^2\sqrt{\frac{\pi}{\lambda k_B T}}\exp\left[-\frac{(\Delta G+\lambda)^2}{4\lambda k_B T}\right] \quad (3)$$

where ΔG is the energy difference between initial and final states of the EET process and for identical molecules, $\Delta G = 0$. λ is the total reorganization energy equaling $\lambda_1 + \lambda_2$, as shown in Figure 1. It measures the intramolecular geometrical

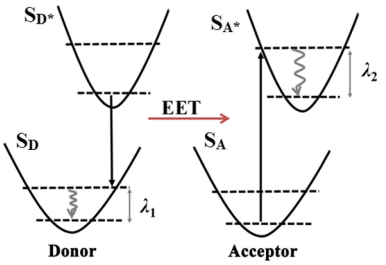

Figure 1. Schematic representation of the energy transfer process from the donor molecule to the acceptor molecule.

organization upon emitting for the donor and absorbing for the acceptor, and represents the stoke shift between the emission of the donor and the absorption of the acceptor. It can also be calculated by summing over all normal modes $\lambda = \sum_j \lambda_j$, where $\lambda_j = S_j\hbar\omega_j$. S_j is the Huang–Rhys factor of the jth mode with frequency ω_j, and it determines the strength of intramolecular vibronic coupling. k_B is the Boltzmann constant. The larger the reorganization energy, the larger the stoke shift, and the smaller the spectral overlap, so EET rates resulting from both FGR and Marcus become smaller as well.

During the exciton diffusion process, the intermolecular energy transfer is proceeded with the competition of intramolecular fluorescent radiative decay (k_r) and non-radiative decay (k_{nr}). The exciton lifetime can be expressed as $\tau = 1/(k_r + k_{nr})$, which is usually ca. 1–10 ns for organic chromophores. The radiative decay rate is determined by the Einstein spontaneous radiation of the transition dipole, which can be expressed as

$$k_r = \int \sigma'_{emi}(\omega)\mathrm{d}\omega \quad (4)$$

where σ' is a dimensionless emission cross section. Also, the non-radiative decay rate from the excited state to the ground state can also be calculated with the FGR by treating non-adiabatic coupling and spin–orbit coupling as perturbation

$$k_{nr} = \frac{2\pi}{\hbar}\sum_{\nu,\mu} P_{i\nu}\left|H'_{f\mu,i\nu} + \sum_{n,\sigma}\frac{H'_{f\mu,n\sigma}H'_{n\sigma,i\nu}}{E_{i\nu} - E_{n\sigma}}\right|^2 \delta(E^f_\mu - E^i_\nu) \quad (5)$$

where P_i is the Boltzmann probability of the initial state (average) and H' is the sum of perturbations from the nuclear kinetic term and spin–orbit coupling, and μ, ν, and σ are indices for vibrational states. The analytic calculation approach for the EET rate with the full quantum effect has been introduced above, whereas the analytic radiative and non-radiative rates have also been derived earlier by us.[26,27,31]

The molecular parameters incorporated in the EET rate and radiative/nonradiative decay rates, such as vibrational normal modes for the ground and excited states as well as vibronic couplings and Duschinsky rotation matrix, are all calculated by density functional theory (DFT). Thus, our approach can be regarded as first-principles because there is no free parameter to adjust.

2.2. Random Walk Simulation Based on the Hopping Model. With all the rates (k's) of possible events, including the rates of EET to another one, the radiative/nonradiative decay, diffusion constant D can be simulated by a random walk simulation. We choose one molecule as the initial exciton center denoted as o. The exciton hops from o to another molecule i with rate k_{eet}^i, in competing with the annihilation process $k_r + k_{nr}$. The hopping probability can be evaluated as $p^i = \frac{k_{eet}^i}{\sum_{i=1}^N k_{eet}^i + k_r + k_{nr}}$, and the simulation time is incremented by $[\sum_{i=1}^N k_{eet}^i]^{-1}$, where N is the total number of exciton-accepting molecules. The larger the number N considered, the longer is the exciton hopping range is taken in simulation. Exciton annihilation can be regarded as the $(N+1)$th event. The hopping distance is taken to be the molecular center–center distance. At each step, a random number r uniformly distributed in $[0, 1]$ is generated. The jth event (exciton hops to the jth molecule or annihilation) will be executed if $\sum_{\alpha=1}^{j-1} p^\alpha < r < \sum_{\alpha=1}^{j} p^\alpha$. If $j = N+1$, the event is either fluorescent decay or nonradiative decay. Then, the simulation will stop and a new simulation will start. Otherwise, the simulation continues until the total simulation time is attained. Such simulations are repeated independently for thousands of times; then, the 3D diffusion coefficient can be obtained as $D = \frac{\langle R^2(t)\rangle}{6t}$, averaging over all trajectories, and the exciton diffusion length is evaluated as $L_D = \sqrt{D\tau}$ finally, where $\langle R^2(t)\rangle$ is the mean-square displacement and τ is the exciton lifetime. The exciton diffusion along a certain direction such as a, b, or c is calculated by projecting the diffusion motion at each step before making the trajectory average.

It should be borne in mind that we have taken the long-range transfer exciton hopping into account here, quantified by N. That is, the hopping can occur from one molecule to any other molecule because the coupling J_{DA} is of long-range character, in sharp contrast to the electron transfer problem where only the nearest neighbor is usually considered. The k_{eet} can be evaluated both by eq 2 with full consideration of the quantum nuclear effect in the spectrum function and by eq 3, where a semiclassical treatment for the spectrum has been employed.

2.3. TDWPD Method. We now go beyond the above-mentioned hopping picture by considering the exciton delocalization effect. We employed a simple tight-binding model here. The effective exciton Hamiltonian considering thermal fluctuations of both the site energy $\varepsilon_{ii}(t)$ and the intermolecular excitonic coupling $\varepsilon_{ij}(t)$ $(i \neq j)$ for organic systems can be expressed as

$$H(t) = \sum_{i=1}^N (\varepsilon_{ii} + F_i(t))|\psi_i\rangle\langle\psi_i| + \sum_{i\neq j}^N (\varepsilon_{ij} + V_{ij}(t))|\psi_i\rangle\langle\psi_j| \quad (6)$$

Here, $|\psi_i\rangle$ corresponds to the excitation state of the ith site. The constant part ε_{ij} in the matrix elements describes the coherent exciton motion in a completely rigid lattice, whereas $F_i(t)$ and $V_{ij}(t)$ represent the fluctuations of exciton site energy and intermolecular excitonic coupling, respectively.

To obtain the memory effect of site energy fluctuation, we need the spectral density function of the exciton–phonon interaction, which can be written as

DOI: 10.1021/acs.jpcc.8b06918
J. Phys. Chem. C 2018, 122, 18365–18375

$$J(\omega) = \frac{\pi}{2}\sum_j \frac{\chi_j^2}{\omega_j}\delta(\omega - \omega_j) \quad (7)$$

Here, the local vibronic coupling strength of the jth normal mode is $\chi_j = \Delta Q_j \omega_j^2$, where ΔQ_j represents the normal-mode coordinate shift between the initial and final states of an energy transfer process. The reorganization energy of the jth normal mode is $\lambda_j = \frac{1}{2\hbar}\Delta Q_j \chi_j$. The δ function is evaluated with Lorentz distribution, $\delta(\omega - \omega_j) = \frac{1}{\pi}\frac{a}{a^2 + (\omega - \omega_j)^2}$. For the sake of simplicity, only the real part of the fluctuation in the correlation function is considered because the particle dynamics caused by the ignorance of imaginary fluctuation has been proven to be small.[23] As a result, the site energy fluctuation can be finally expressed as

$$F_i(t) = \sum_{n=1}^{N} [2G(\omega_n)\Delta\omega]^{1/2} \cos(\omega_n t + \phi_n) \quad (8)$$

Here, $G(\omega) = J(\omega)\coth(\beta^T\omega/2)/\pi$ is the modified spectral density function at a special temperature T ($\beta = 1/k_B T$) to make it satisfy the detailed balance condition; $\Delta\omega = \omega_{max}/N$, where ω_{max} is the upper cutoff frequency, and $\omega_n = n\Delta\omega$. ϕ_n is a random phase uniformly distributed over the interval $[0, 2\pi]$.

To describe the exciton dynamics, the time-dependent Schrödinger equation is solved with the Chebyshev polynomial expansion technique.[32,33] Once the wave function of the system, $\psi(t) = \sum_i^N c_i(t)|i\rangle$, is known, the time-dependent properties of exciton can be easily obtained. The 3D diffusion coefficient can also be obtained by $D = \lim_{t\to\infty} \frac{\langle R^2(t)\rangle}{6t}$, where $\langle R^2(t)\rangle = \sum_i^N r_i^2 \rho_{ii}(t)$ will grow linearly with time t after some time. The origin is defined as $\langle R^2(0)\rangle = 0$ with one exciton completely localized on one site a. r_i is the distance from site i to site a, and $\rho_{ii}(t) = \langle c_i^*(t)c_i(t)\rangle$ is the exciton population on site i, which averages over a few hundred trajectories. The exciton diffusion along a chosen direction happens by projecting the diffusion motion at each step before trajectory average.

2.4. Computational Procedures. In order to contain the environmental effects in computing the photophysical properties of crystals, QM/MM calculations have been carried out for geometry optimizations, vibrational frequencies, dipole transitions, and so forth, by using ChemShell 3.4 interface package.[34] The QM/MM models are built up by cutting out a cluster from the X-ray crystal structures (see the Supporting Information, Table S1) and setting the central molecule as a QM part while its surroundings as an MM part. The QM/MM cluster size is 3 M part3 for both systems, which is enough for considering the environmental effect for a single site. The geometry optimizations are performed by the hybrid delocalized internal coordinate optimizer, with the QM molecule active and MM molecules frozen. Turbomole 6.3 and DL-POLY program package[35] were used to calculate the energies and gradients of QM and MM molecules, respectively. (TD)B3LYP/6-31G(d) is used for QM calculations. The MM parts are treated with the general Amber force field,[36] and the QM/MM interactions are described by the electrostatic embedding scheme.[37] On the basis of the optimized geometries and corresponding frequency analyses at the ground and the lowest excited states (S_0 and S_1), the vibronic couplings and reorganization energies of all normal modes are obtained by the DUSHIN program.[38] Then, the analytical Franck−Condon integrals of absorption and emission as well as the fluorescent/nonradiative decay rate via TVCF formalism are calculated by using the MOMAP program.[39] In addition, excitonic couplings are calculated with the direct coupling method[40] by using the analytical integration routine via the MOMAP program coupled with NWchem6.5 package,[41] and the full time-dependent (TD) DFT method combined with B3LYP/6-31G(d) is used. For the random walk simulations, 8000 trajectories have been computed independently for getting the mean-square displacement. The model Hamiltonians for TDWPD calculations are based on an 11 1 tonia11 cluster with 3146 molecules for anthracene and an 11 1 clust11 cluster with 4356 molecules for BF2bcz, and 400 trajectories are repeated for achieving the mean-square displacement. All simulations are performed at a temperature of 300 K.

3. RESULTS AND DISCUSSION

3.1. Optical Spectra and Excited-State Decay Rates in Anthracene and BF_2bcz Crystals. After optimizing the S_0 and S_1 geometries, the corresponding frequencies have been analytically solved. Then, the reorganization energies of all normal modes have been calculated. On the basis of the reorganization energy distributions, the analytical Franck−Condon integrals of absorption and emission with the temperature effect and full quantum effect (namely, considering all normal modes with infinite vibrational quanta) have been solved by applying TVCF formalisms and are depicted in Figure 2 in comparison with the experimental data.[29,42] In addition, the fluorescent decay rate (k_f) and the nonradiative internal conversion decay rate (k_{ic}) have been computed by using the TVCF method while considering the Duschinsky rotation effect and are listed in Table 1. The corresponding experimental data have also been presented in Table 1 for comparison.

For anthracene, TDDFT calculations give the maxima of absorption and emission as 425 and 426 nm, respectively, which are close to the experimental data as 393 and 400 nm (Table 1). Such a small stokes shift in anthracene is mainly caused by its rigid conjugated molecular structure, which can cause little displacement between S_0 and S_1. Besides, because of the conjugated structure, k_{ic} (0.52×10^2 s^{-1}) in anthracene is much smaller than k_f (1.85×10^7 s^{-1}), showing good agreement with the experiment. It should be noted that both experimental and theoretical results show that the intersystem crossing (ISC) decay $S_1 \rightarrow T_2$ plays a significant role in competition with the $S_1 \rightarrow S_0$ decay process,[43,44] and the k_{isc} of $S_1 \rightarrow T_2$ obtained from our TCVF method is 2.6×10^7 s^{-1}, which is larger than the calculated k_f, finally leading to 22.47 ns of singlet exciton lifetime and 42% of fluorescent quantum yield. For BF_2bcz, because no absorption spectrum and decay rate have been measured in crystal, we list these experimental data measured in acetone solution in Table 1 for reference. The theoretical emission agrees well with experimental fluorescence of crystal in both maximum and shape. In addition, k_{ic} is of the order of 10^7 s^{-1}, which is again coincidental with the experiment. The relatively larger value of k_f also agrees with the experiment. No ISC decay has been discovered in difluoroboron β-diketonate derivatives, so the singlet exciton lifetime and the fluorescent quantum yield are derived as 17.98 ns and 74%, respectively.

3.2. Long-Distance Hopping Effect on Energy Transfer. We now look at the long-range energy transfer effect on

DOI: 10.1021/acs.jpcc.8b06918
J. Phys. Chem. C 2018, 122, 18365−18375

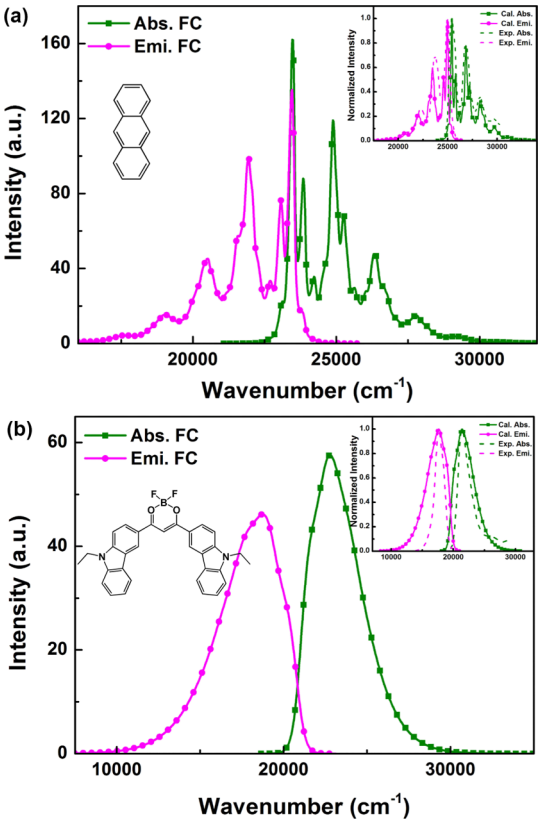

Figure 2. Theoretical absorption and emission spectra for (a) anthracene and (b) BF_2bcz crystals. The normalized theoretical and experimental absorption and emission spectra have been shown in the inset, and the theoretical absorption/emission spectra have been shifted to match the experimental peaks by 1916/1526 cm^{-1} for anthracene and 1285/1374 cm^{-1} for BF_2bcz. A Lorentz broadening factor of 100 cm^{-1} is added to eliminate the sharp oscillation in theoretical spectra for anthracene. The experimental absorption of BF_2bcz is measured in CH_2Cl_2 solution, whereas that of other experiments are all measured in crystal.

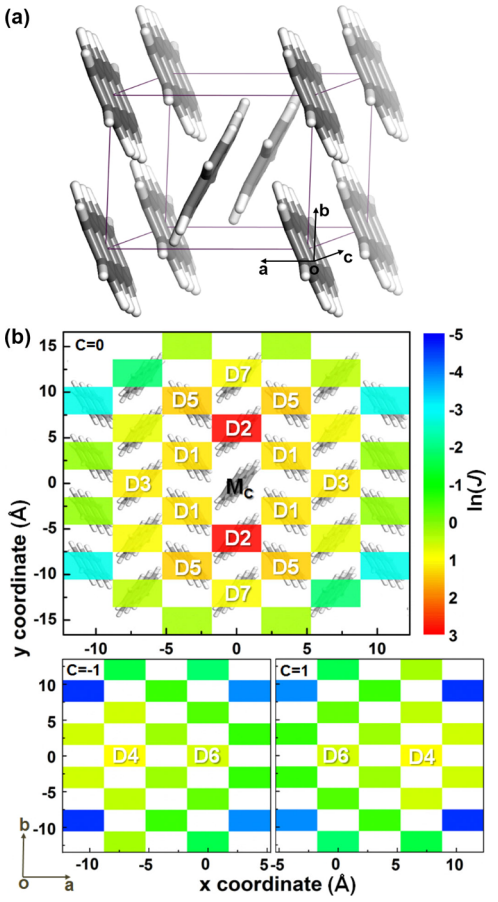

Figure 3. (a) Crystal structure of the unit cell and (b) the ab planar 2D map of the excitonic couplings between the center molecule (M_C) and others in the same plane ($C = 0$) and in the two adjacent planes ($C = \pm 1$) for anthracene.

the exciton diffusion in anthracene. EET can occur over a long distance (typically in the range of 1−10 nm) because of the long-range Coulomb interaction contributing to the excitonic coupling. Thus, a total number of ∼150 coupling pairs between two molecules have been considered in the case of the anthracene crystal, and the selected pairs are plotted as shown in Figure 3 according to the coupling values, all of which are within the same *ab* plane or between two adjacent *ab* planes. By the way, for validating our excitonic coupling calculation, the excitonic couplings have also been computed by Q-Chem software[48] at the same level. The coincident values shown in Table S2 interpret the accuracy of our program. The coupling values and centroid distances of major EET paths are presented in Table 2. It is obvious that the coupling in the *b* direction (D2) is much stronger than in other directions, whereas the couplings in the *c* direction are very weak, indicating that the sequence of directional diffusion capability is $b > a > c$. As the intermolecular spacing distance increases, the excitonic coupling decreases sharply. For example, the EET acceptor changes from D2 to D7, the reduction of coupling is nearly proportional to R^3 with the unchanged molecular reorientation, which fits the dipole−dipole model.[9] The total reorganization energy obtained from the normal modes analysis amounts to 420.0 meV, which is much larger than the largest intermolecular excitonic coupling (18.6 meV), implying a completely incoherent energy transport mechanism.

Table 1. Theoretical and Experimental Absorption and Emission Maxima (λ_{abs} and λ_{emi}), the Fluorescent Decay Rate (k_f), the Internal Conversion Decay Rate (k_{ic}), the Intersystem Crossing Rate (k_{isc}), the Singlet Exciton Lifetime (τ), and the Fluorescent Quantum Yield (Φ_f) for Anthracene and BF2bcz Crystals

		λ_{abs}(nm)	λ_{emi} (nm)	k_f (s^{-1})	k_{ic} (s^{-1})	k_{isc} (s^{-1})	τ (ns)	Φ_f (%)
Anth.	Cal.	425	426	1.85×10^7	0.52×10^2	2.6×10^7[a]	22.47	42
	Exp.	393[b]	400[b]	$0.71–2.9 \times 10^8$,[c] 6.20×10^7[d,h]	3.50×10^5[d,h]	$1.51 \times .10^8$[d,h]	10−15[e], 4.69[d,h]	29[d,h]
BF_2bcz	Cal.	437	526	4.12×10^7	1.44×10^7	n.a.	17.98	74
	Exp.	463[f,h]	567[f,g], 506[f,h]	3.3×10^8[f,h]	8.0×10^7[f,h]	n.a.	3.25[g], 2.45[f,h]	37[f], 81[f,h]

[a]Reference 43. [b]Reference 42. [c]Reference 45. [d]Reference 44. [e]Reference 46. [f]Reference 47. [g]Reference 29. [h]The experimental data for anthracene were measured in cyclohexane solution, and the data for BF2bcz were measured in acetone solution.

DOI: 10.1021/acs.jpcc.8b06918
J. Phys. Chem. C 2018, 122, 18365−18375

Table 2. Centroid Distances (R), Excitonic Couplings (J), FGR Rates (k_{FGR}), as Well as Marcus Rates (k_{Marcus}) between Selected Dimers (D1−D7) in the Anthracene Crystal as Labeled in Figure 3b[a]

dimers	R (Å)	J (meV)	k_{FGR} (s^{-1})	k_{Marcus} (s^{-1})
D1	5.24	3.43	1.62×10^{11}	5.24×10^{9}
D2	6.04	18.58	4.77×10^{12}	1.54×10^{11}
D3	8.56	3.14	1.36×10^{11}	4.39×10^{9}
D4	9.45	2.65	9.70×10^{10}	3.12×10^{9}
D5	10.02	4.06	2.28×10^{11}	7.34×10^{9}
D6	11.18	1.90	4.99×10^{10}	1.61×10^{9}
D7	12.08	2.52	8.64×10^{10}	2.83×10^{9}
λ_{reorg} = 420.0 meV				

[a]The total reorganization energy (λ_{reorg}) has also been given.

With the reorganization energy, the Marcus rates are computed with eq 3 and listed in Table 2 as well. Moreover, combined with the calculated Franck−Condon integrals of absorption and emission, the FGR rates are also calculated via eq 2. Even though the excitonic couplings are relatively low compared to other organic molecular crystals,[49] the largest FGR rate in the anthracene crystal can still reach the order of 10^{12} s^{-1}, which should be ascribed to the large spectra overlap.

With the calculated EET rates as well as the exciton decay rates (k_f, k_{ic}, and k_{isc}), the 3D singlet exciton diffusion processes depending on both FGR and Marcus theories are simulated by KMC. For comparison, the TDWPD method, which contains both the quantum nuclear effect and the exciton delocalization effect, has also been used to simulate the 3D exciton motion in the anthracene crystal. In order to discuss the long-range effect on the exciton diffusion, we take a series of simulations with the total number of exciton-accepting molecules ranging from 16 to 150, by setting the cutoff value of the nearest atomic spacing between two molecules from 5 to 14.6 Å. The 3D-average exciton diffusion coefficients computed by three different methods show a similar increasing tendency along with increasing cutoff values (Table S3). The theoretical exciton diffusion lengths at the cutoffs of 5, 10, and 14.6 Å separately are listed in Table 3. All three methods predict ca. 30 and 5% increases on the 3D-average diffusion length by enlarging the cutoff value from 5 to 10 Å and from 10 to 14.6 Å, respectively, indicating a relatively weak long-range effect on the 3D-average exciton diffusion. By projecting the diffusion along a, b, and c directions, the directional exciton diffusion lengths can be obtained. The exciton diffusion in the b direction makes the major contribution to 3D-average diffusion, and the increase of the corresponding diffusion length is only ca. 17%, with hopping cutoff enhancing from 5 to 10 Å as predicted by FGR, presenting a weak long-range effect as well. However, for the directional exciton diffusions along a and c axes with a relatively small contribution to 3D-average diffusion, it shows a strong long-range effect such that the diffusion lengths increased ca. 145 and 66% separately by enhancing the cutoff from 5 to 10 Å (Figure 4). Furthermore, if only 16 neighboring accepting molecules are included, the predicted relation between three directional diffusion lengths along the axes ($b > c > a$) is mismatched with the experiment ($b > a > c$). Therefore, we consider that the long-range effect is more important on the directional exciton diffusion than on 3D-average diffusion, especially on the direction with relatively weak diffusion capability. Besides, for both 3D-average and directional diffusion properties, the exciton diffusion coefficients start to converge when the cutoff value of atomic spacing rises up to 10 Å, providing a reference for the following investigations.

Table 3. Calculated 3D-Averaged Exciton Diffusion Lengths As Well As along a, b, and c Axes Obtained by Marcus Theory, FGR Theory, and TDWPD Method at Three Different Cutoff Values (Å) in the Anthracene Crystal[a]

cutoff (Å)	Marcus (nm)	FGR (nm)	TDWPD (nm)
5	**3D: 21.9**	**3D: 121.9**	**3D: 140.8**
	a: 7.9	a: 43.5	a: 52.3
	b: 35.9	b: 200.4	b: 230.3
	c: 10.0	c: 55.1	c: 66.6
10	**3D: 28.4**	**3D: 157.9**	**3D: 186.6**
	a: 19.5	a: 108.4	a: 127.9
	b: 42.1	b: 234.5	b: 276.8
	c: 16.6	c: 91.4	c: 110.8
14.6	**3D: 30.0**	**3D: 166.9**	**3D: 194.9**
	a: 20.9	a: 116.9	a: 139.4
	b: 44.1	b: 245.6	b: 282.9
	c: 18.4	c: 101.9	c: 124.2
Exp. a: 60 ± 10[b]			
b: ∼100[b]			
c: 36 ± 20[b], 47 ± 1[c], 49 ± 1[c], 60 ± 5[d]			

[a]The experimental results are also given for comparison. [b]Reference 42. [c]Reference 7. [d]Reference 50.

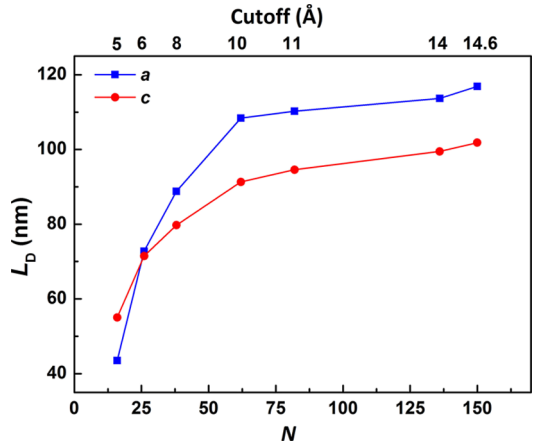

Figure 4. Theoretical exciton diffusion lengths along a and c axes evaluated by the FGR method for anthracene as a function of the number of accepting molecules N and the corresponding hopping distance cutoff.

We then study the exciton diffusion property in BF_2bcz with distance cutoff values of 5 and 10 Å, amounting to 18 and 42 exciton-accepting molecules. The 2D distribution of theoretical excitonic couplings is shown in Figure 5, and the excitonic coupling values, the corresponding centroid distances of major dimers, and the EET rates calculated by both FGR and Marcus theories are listed in Table 4. The diffusion lengths are evaluated by two hopping models as well as the TDWPD method (Table 5). By enlarging the cutoff from 5 to 10 Å, the 3D-average exciton diffusion length is increased by ca. 25% only, whereas the directional diffusion length along the b axis, which is the smallest among the three axes, is increased by ca. 80%, showing a similar long-range effect as the anthracene system. Thus, we believe that the long-range effect should play an essential role in the directional exciton diffusion with

DOI: 10.1021/acs.jpcc.8b06918
J. Phys. Chem. C 2018, 122, 18365−18375

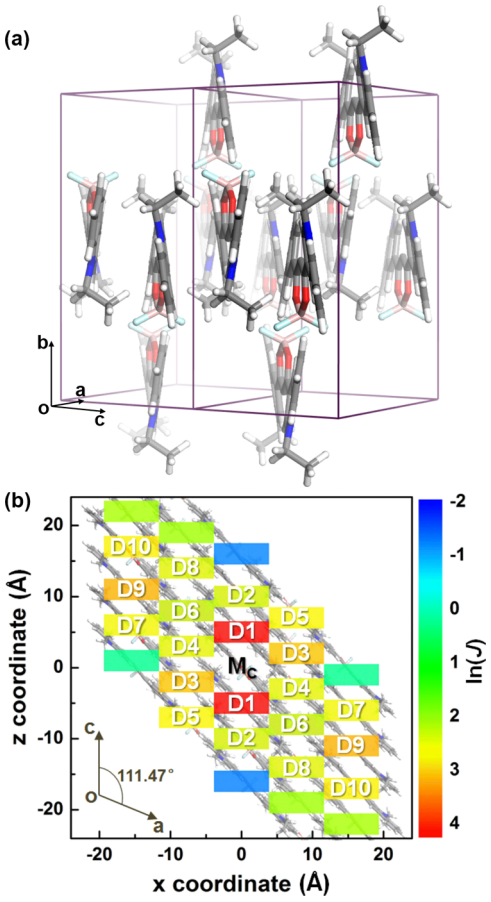

Figure 5. (a) Crystal structure of the unit cell and the (b) *ac* planar 2D map of the excitonic couplings between the central molecule (M_C) and others in the same plane (B = 0, containing D1, D2, D7, D9, and D10) or in adjacent *ac* planes (B = −1/2, containing D3−D6, and D8) for BF_2bcz.

Table 4. Centroid Distances (R), Excitonic Couplings (J), FGR Rates (k_{FGR}), As Well As Marcus Rates (k_{Marcus}) between Selected Dimers (D1−D10) in the BF_2bcz Crystal as Labeled in Figure 5b[a]

dimers	R (Å)	J (meV)	k_{FGR} (s^{-1})	k_{Marcus} (s^{-1})
D1	5.24	69.95	1.39×10^{12}	1.97×10^{11}
D2	10.43	11.39	3.68×10^{10}	5.21×10^{9}
D3	11.56	22.38	1.42×10^{11}	2.01×10^{10}
D4	12.04	12.34	4.31×10^{10}	6.11×10^{9}
D5	13.82	14.82	6.23×10^{10}	8.82×10^{9}
D6	14.05	10.33	3.01×10^{10}	4.30×10^{9}
D7	16.63	13.30	5.02×10^{10}	7.11×10^{9}
D8	17.85	12.00	4.08×10^{10}	5.78×10^{9}
D9	19.18	25.11	1.79×10^{11}	2.53×10^{10}
D10	22.68	17.47	8.66×10^{10}	1.23×10^{10}
		λ_{reorg} = 646.4 meV		

[a]The total reorganization energy (λ_{reorg}) has also been given.

relatively weak diffusion capability, but is not very significant in the 3D-averaged exciton diffusion.

3.3. Quantum Nuclear and Delocalization Effects on Energy Transfer. The results from the Marcus theory show that the diffusion length of BF_2bcz doubles that of anthracene because of the much smaller excitonic couplings in anthracene, even though the total reorganization energy in anthracene is

Table 5. Exciton Diffusion Lengths Given in 3D-Averaged and along *a*, *b*, and *c* Axes, Obtained by Marcus Model, FGR Theory, As Well As TDWPD Method for the BF_2bcz Crystal with Cutoff Hopping Distances of 5 and 10 Å[a]

cutoff (Å)	Marcus (nm)	FGR (nm)	TDWPD (nm)
5	**3D: 40.8**	**3D: 107.9**	**3D: 693.6**
	a: 56.7	*a*: 149.1	*a*: 970.4
	b: 20.0	*b*: 53.8	*b*: 379.0
	c: 51.5	*c*: 136.1	*c*: 800.4
10	**3D: 51.0**	**3D: 134.5**	**3D: 861.2**
	a: 65.4	*a*: 171.4	*a*: 1113.0
	b: 36.8	*b*: 97.9	*b*: 685.6
	c: 59.1	*c*: 155.3	*c*: 915.4
		Exp. >100	

[a]The estimated experimental L_D is also given for comparison.

only two-third of that in BF_2bcz. For both anthracene and BF_2bcz, the sequence of exciton diffusion lengths obtained from the three approaches is as follows: $L_{TDWPD} > L_{Quantum} > L_{Marcus}$. It is natural that both the quantum nuclear effect and the exciton delocalization or coherence can facilitate exciton diffusion. In the Marcus theory, the short-time and high-temperature approximations eliminate the quantum effect of nuclear vibrations and reach the semiclassical limit. The calculated EET rates listed in Tables 2 and 4 show that the FGR rate is 30 times over the Marcus rate for anthracene and 7 times for BF_2bcz, indicating that the lack of the quantum nuclear effect will diminish the theoretical EET rate. When comparing with experimental results, we find that the Marcus theory dramatically underestimates the exciton diffusion lengths for the two systems, whereas both the quantum hopping model and the TDWPD method can give reasonable results in agreement with experiments. This confirms the existence and significance of the nuclear quantum effect on the exciton diffusion process.

In order to get a deeper understanding of the nuclear quantum effects, especially the relation with molecular structures, we plot the Huang−Rhys factor distributions to normal modes for the two systems as shown in Figure 6a,b. The Franck−Condon factor actually can be expressed as FC = $\sum_{\nu_f}\prod_k |\langle\chi_{f\nu_k}|\chi_{i0}\rangle|^2$ under the harmonic oscillator model $|\Theta_{f\nu_f}\rangle = |\chi_{f\nu_f}\chi_{f\nu_{f2}}\cdots\chi_{f\nu_{fN}}\rangle$, and $|\langle\chi_{f\nu_k}|\chi_{i0}\rangle|^2 = \frac{S_k^{\nu_k}}{\nu_k!}e^{-S_k}$, where ν_k is the vibrational quantum number of the kth normal mode. In order to distinguish the cause of different nuclear quantum effects in the two systems, we also calculate the spectra at 0 K under the displaced harmonic oscillator model by the sum-over-state method (Figure 6c,d). The major transitions related to normal modes have also been labeled. For each spectrum, it is easy to find that the larger the Huang−Rhys factor a normal mode has, the more contribution to Franck−Condon intensity it has. Through comparison with the analytical spectra at 300 K, we find that the overlapped spectrum in anthracene is mainly contributed by 0−0 transition. The dominated normal modes of anthracene are in-plane bending (mode 6 for S_0) and conjugated C−C stretching vibrations (modes 48 and 53 for S_0) (Figure S1) because of its perfect conjugated geometry, and the vibrations with low frequency contribute less to the transition. All Huang−Rhys factors of normal modes are no more than 0.5, so that it is mainly the vibrations with first quantum to accept or emit the excitation energy. Thus, the spectra of anthracene possess narrow peaks with relatively high

DOI: 10.1021/acs.jpcc.8b06918
J. Phys. Chem. C 2018, 122, 18365−18375

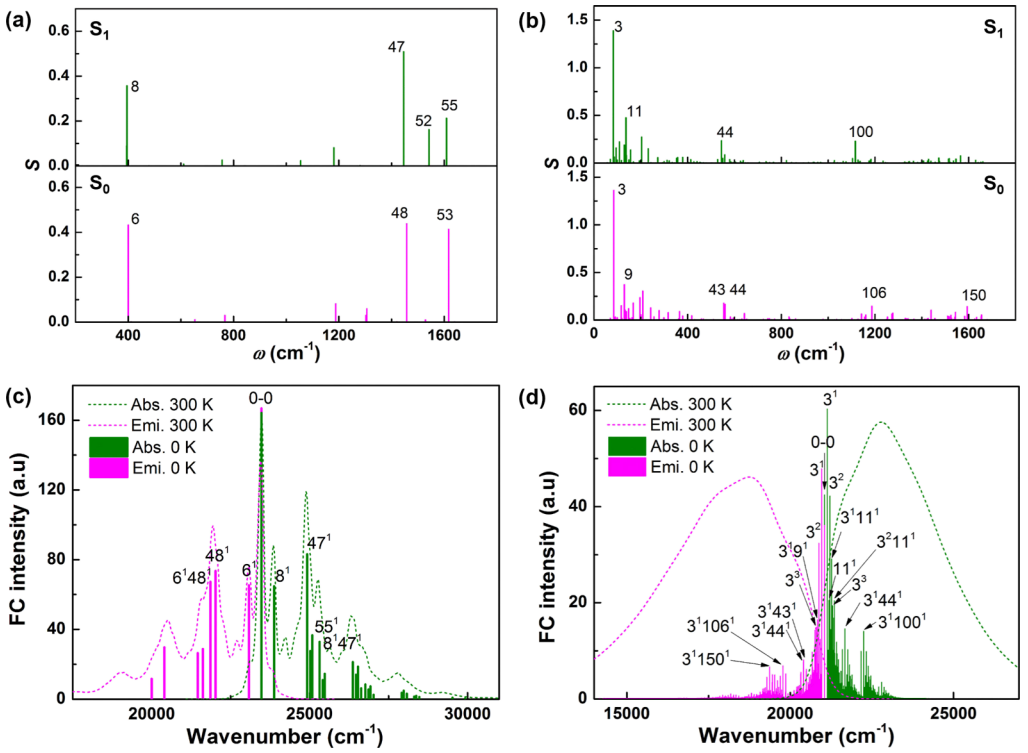

Figure 6. Huang–Rhys factor (S) distributions to all normal modes for (a) anthracene and (b) BF_2bcz; the index of dominated normal modes are labeled. The Franck–Condon spectra (columns for T = 0 K, dash for T = 300 K) and their assignments of transition are labeled as N^{ν} (N is the index of normal modes and ν is the quantum number) for (c) anthracene and (d) BF_2bcz. The dominated normal modes for anthracene and BF_2bcz have been drawn in Figure S1.

intensity. As for BF_2bcz, besides the 0–0 transition, the low-frequency rotation vibrations (~100 cm^{-1}) with the high Huang–Rhys factor (modes **3** and **9** for S_0) also make a certain contribution to the spectral overlapped part. The Huang–Rhys factor of the normal mode 3 is as large as 1.4 so that more quanta (1, 2, 3, ...) will participate in the transition process; then, the spectrum is broadened and the Franck–Condon intensity of peak is lowered. Furthermore, the contribution of low-frequency modes will become weak when temperature rises up to 300 K because of the Boltzmann distribution. Thus, the spectra overlap, which contains the nuclear quantum effect, is much smaller in BF_2bcz compared to anthracene.

The TDWPD approach contains both the quantum nature of nuclear motion through the harmonic oscillator model and the exciton delocalization as well as coherence. It is seen from Tables 3 and 5 that the exciton diffusion lengths obtained by the TDWPD method are always larger than the results from the quantum hopping model. For anthracene, the 3D-averaged exciton diffusion lengths predicted by quantum hopping and TDWPD methods are both of the order of 100 nm, whereas for BF2bcz, it becomes as long as 861 nm, much longer than the quantum hopping result (134 nm). The coherence effect usually can be simply visualized by the oscillation behavior in the exciton population propagation on the initial site. As shown in Figure S2, for both anthracene and BF2bcz, there does not exist any appreciable oscillation behavior for the $\rho_{oo}(t)-t$ curve, indicating that the exciton coherence can be ignored. Moreover, the quasi-thermal-equilibrium of diffusion can be obtained very efficiently, as seen in Figure S3. The exciton delocalization on the *ab* plane for anthracene and on the *ac* plane for BF2bcz at 24 fs is illustrated in Figure 7. It is seen that the exciton in anthracene is still almost localized on

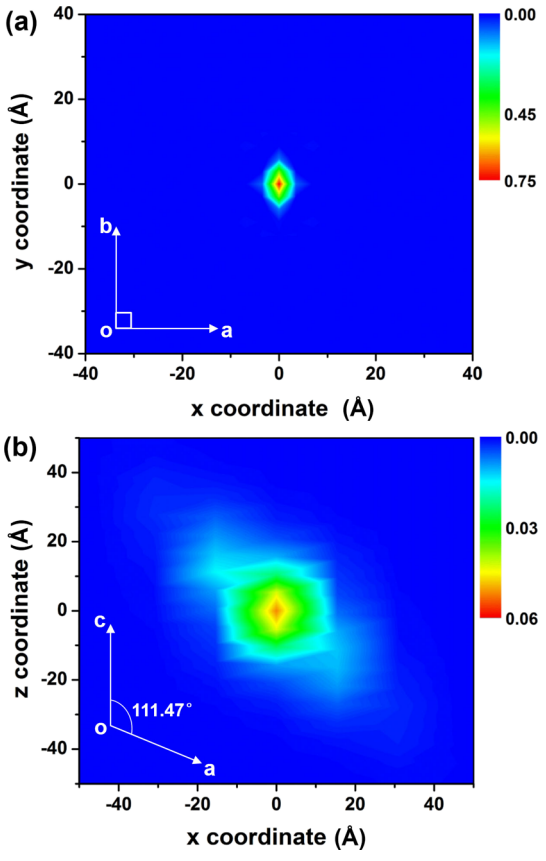

Figure 7. Exciton population distributions of (a) anthracene and (b) BF_2bcz at 24 fs.

DOI: 10.1021/acs.jpcc.8b06918
J. Phys. Chem. C 2018, 122, 18365–18375

the initial site, whereas the exciton in BF2bcz is well delocalized. The exciton delocalization lengths estimated as $L = \sqrt{1/\sum \rho_{ii}^2}$ [20] are calculated to be 1.3 and 9.2 for anthracene and BF2bcz, respectively. That is, the exciton can be viewed as localized on one molecule in anthracene and delocalized over nine molecules in BF_2bcz. Such a difference between anthracene and BF_2bcz can be rationalized by the ratio of excitonic coupling over vibronic coupling J/λ: about 0.04 for anthracene and 0.1 for BF_2bcz (cf. Tables 2 and 4). Thus, for anthracene, the values of the exciton diffusion length obtained from quantum hopping and TDWPD methods are close to each other and an incoherent but long-range hopping picture is more relevant. On the other hand, the TDWPD method should be more appropriate to describe ultralong exciton diffusion, such as the BF_2bcz system. The calculated results indicate that BF_2bcz is a promising candidate to apply in photovoltaics and other light-harvesting devices.

4. CONCLUSIONS

To summarize, we have investigated the intrinsic exciton diffusion property in OSCs at three levels ranging from the semiclassical hopping model based on the Marcus theory, to the quantum nuclear tunneling−mediated hopping, and then to the TDWPD approach. The semiclassical Marcus theory treats nuclear vibrations classical, whereas FGR considers the quantum nuclear effect accompanying the exciton hopping process. TDWPD can effectively consider the exciton delocalization effect in addition to the quantum nuclear effect. A multiscale simulation approach is developed to calculate the exciton diffusion length starting from the first-principles evaluated molecular photophysical parameters, such as the radiative/nonradiative decay rate, the optical spectra, and energy transfer rates, all of which can be obtained by the TVCF approach that we developed earlier. Besides, the long-range hopping processes are taken into consideration.

For anthracene and BF_2bcz crystals, the calculated photophysical properties are in good agreement with experiments, providing a solid basis for the exciton diffusion simulations. We then investigated the long-range energy transfer effect, which has been mostly ignored. It was found that the long-range energy transfer plays a more important role in the directional exciton diffusion rather than in 3D-averaged diffusion. Especially for anthracene, when only 16 nearest accepting molecules are included in simulations, the exciton diffusion along the *a* axis will be underestimated ca. 60%, and the relation between diffusion lengths along *a* and *c* axes is predicted in a wrong order. For both anthracene and BF_2bcz, the 3D-averaged and directional exciton diffusion lengths begin to converge after the hopping cutoff of the nearest intermolecular atomic spacing reach 10 Å. By comparison with experimental results, the semiclassical Marcus theory underestimates the exciton diffusion lengths for both systems because of the ignorance of the nuclear quantum effect. In contrast, both the quantum hopping model and the TDWPD method can give appropriate descriptions, implying the universality of nuclear tunneling−assisted exciton diffusion in OSCs. The rotation vibrations with low frequency and high vibronic coupling in BF_2bcz lead to a weaker quantum nuclear effect compared to anthracene. Besides, TDWPD calculations demonstrate that the delocalization effect plays an important role in facilitating the transport. For the BF2bcz system, where the exciton delocalization effect is relatively strong, the wave packet description with the quantum nuclear effect is more appropriate, and the ultralong distance in exciton diffusion can be revealed. For the anthracene system with a weak delocalization effect, a simple nuclear tunneling−enabled hopping model is sufficient.

■ ASSOCIATED CONTENT

Supporting Information

The Supporting Information is available free of charge on the ACS Publications website at DOI: 10.1021/acs.jpcc.8b06918.

Unit cell parameters for the molecular crystals, the calculated excitonic couplings for all of the selected dimers (D1−D7), the 3D-averaged exciton diffusion coefficients at the three levels, and the dominant intramolecular vibrational modes coupled with exciton, TDWPD-simulated exciton population and diffusion processes (PDF)

■ AUTHOR INFORMATION

Corresponding Authors

*E-mail: jiangyq@nanoctr.cn (Y.J.).
*E-mail: zgshuai@tsinghua.edu.cn (Z.S.).

ORCID

Yuqian Jiang: 0000-0002-7013-4704
Zhigang Shuai: 0000-0003-3867-2331
Minghua Liu: 0000-0002-6603-1251

Notes

The authors declare no competing financial interest.

■ ACKNOWLEDGMENTS

The authors are grateful to Prof. Yi Zhao of Xiamen University for his help in using the TDWPD method. This work is supported by the National Natural Science Foundation of China (grant no. 21603043). Z.S. is supported by the NSFC Science Center on Luminescence from Molecular Aggregates (CELMA) grant no. 21788102. Numerical calculations have been performed in Tsinghua University high-performance computation center.

■ REFERENCES

(1) Brédas, J.-L.; Sargent, E. H.; Scholes, G. D. Photovoltaic concepts inspired by coherence effects in photosynthetic systems. *Nat. Mater.* **2016**, *16*, 35.
(2) Hedley, G. J.; Ruseckas, A.; Samuel, I. D. W. Light Harvesting for Organic Photovoltaics. *Chem. Rev.* **2017**, *117*, 796−837.
(3) Scholes, G. D.; Rumbles, G. Excitons in nanoscale systems. *Nat. Mater.* **2006**, *5*, 683−696.
(4) Menke, S. M.; Holmes, R. J. Exciton diffusion in organic photovoltaic cells. *Energy Environ. Sci.* **2014**, *7*, 499−512.
(5) Kozlov, O. V.; de Haan, F.; Kerner, R. A.; Rand, B. P.; Cheyns, D.; Pshenichnikov, M. S. Real-Time Tracking of Singlet Exciton Diffusion in Organic Semiconductors. *Phys. Rev. Lett.* **2016**, *116*, 5.
(6) Lunt, R. R.; Giebink, N. C.; Belak, A. A.; Benziger, J. B.; Forrest, S. R. Exciton diffusion lengths of organic semiconductor thin films measured by spectrally resolved photoluminescence quenching. *J. Appl. Phys.* **2009**, *105*, 053711.
(7) Cohen, M. D.; Klein, E.; Ludmer, Z. Micromeasurements of exciton diffusion lengths in single crystals of anthracene. *Chem. Phys. Lett.* **1976**, *37*, 611−613.
(8) Haedler, A. T.; Kreger, K.; Issac, A.; Wittmann, B.; Kivala, M.; Hammer, N.; Köhler, J.; Schmidt, H.-W.; Hildner, R. Long-range energy transport in single supramolecular nanofibres at room temperature. *Nature* **2015**, *523*, 196−199.

DOI: 10.1021/acs.jpcc.8b06918
J. Phys. Chem. C 2018, 122, 18365−18375

(9) Scholes, G. D. LONG-RANGERESONANCEENERGYTRANSFER INMOLECULARSYSTEMS. *Annu. Rev. Phys. Chem.* **2003**, *54*, 57−87.
(10) Madigan, C.; Bulović, V. Modeling of Exciton Diffusion in Amorphous Organic Thin Films. *Phys. Rev. Lett.* **2006**, *96*, 046404.
(11) Stehr, V.; Fink, R. F.; Engels, B.; Pflaum, J.; Deibel, C. Singlet Exciton Diffusion in Organic Crystals Based on Marcus Transfer Rates. *J. Chem. Theory Comput.* **2014**, *10*, 1242−1255.
(12) Si, Y.; Yang, B.; Qin, H.; Yuan, J.; Wang, S.; Chen, H.; Zhao, Y. Atomistic Modeling of Triplet−Triplet Energy-Transfer Rates from Drug (S)-Propranolol to (R)-Cinacalcet in Human α1-Acid Glycoprotein. *J. Phys. Chem. C* **2015**, *119*, 8014−8022.
(13) Athanasopoulos, S.; Emelianova, E. V.; Walker, A. B.; Beljonne, D. Exciton diffusion in energetically disordered organic materials. *Phys. Rev. B: Condens. Matter Mater. Phys.* **2009**, *80*, 195209.
(14) Hennebicq, E.; Pourtois, G.; Scholes, G. D.; Herz, L. M.; Russell, D. M.; Silva, C.; Setayesh, S.; Grimsdale, A. C.; Müllen, K.; Brédas, J.-L.; Beljonne, D. Exciton Migration in Rigid-Rod Conjugated Polymers: An Improved Förster Model. *J. Am. Chem. Soc.* **2005**, *127*, 4744−4762.
(15) Stehr, V.; Engels, B.; Deibel, C.; Fink, R. F. Anisotropy of singlet exciton diffusion in organic semiconductor crystals from ab initio approaches. *J. Chem. Phys.* **2014**, *140*, 024503.
(16) Jiang, Y.; Zhong, X.; Shi, W.; Peng, Q.; Geng, H.; Zhao, Y.; Shuai, Z. Nuclear quantum tunnelling and carrier delocalization effects to bridge the gap between hopping and bandlike behaviors in organic semiconductors. *Nanoscale Horiz.* **2016**, *1*, 53−59.
(17) Nan, G.; Yang, X.; Wang, L.; Shuai, Z.; Zhao, Y. Nuclear tunneling effects of charge transport in rubrene, tetracene, and pentacene. *Phys. Rev. B: Condens. Matter Mater. Phys.* **2009**, *79*, 115203.
(18) Sung, J.; Kim, P.; Fimmel, B.; Würthner, F.; Kim, D. Direct observation of ultrafast coherent exciton dynamics in helical π-stacks of self-assembled perylene bisimides. *Nat. Commun.* **2015**, *6*, 8646.
(19) Wan, Y.; Stradomska, A.; Knoester, J.; Huang, L. Direct Imaging of Exciton Transport in Tubular Porphyrin Aggregates by Ultrafast Microscopy. *J. Am. Chem. Soc.* **2017**, *139*, 7287−7293.
(20) Chuang, C.; Lee, C. K.; Moix, J. M.; Knoester, J.; Cao, J. S. Quantum Diffusion on Molecular Tubes: Universal Scaling of the 1D to 2D Transition. *Phys. Rev. Lett.* **2016**, *116*, 196803.
(21) Valleau, S.; Saikin, S. K.; Yung, M.-H.; Guzik, A. A. Exciton transport in thin-film cyanine dye J-aggregates. *J. Chem. Phys.* **2012**, *137*, 034109.
(22) Fornari, R. P.; Aragó, J.; Troisi, A. Exciton Dynamics in Phthalocyanine Molecular Crystals. *J. Phys. Chem. C* **2016**, *120*, 7987−7996.
(23) Zhong, X.; Zhao, Y. Charge carrier dynamics in phonon-induced fluctuation systems from time-dependent wavepacket diffusion approach. *J. Chem. Phys.* **2011**, *135*, 134110.
(24) Han, L.; Zhong, X.; Liang, W.; Zhao, Y. Energy relaxation and separation of a hot electron-hole pair in organic aggregates from a time-dependent wavepacket diffusion method. *J. Chem. Phys.* **2014**, *140*, 214107.
(25) Jing, Y.; Chen, L.; Bai, S.; Shi, Q. Equilibrium excited state and emission spectra of molecular aggregates from the hierarchical equations of motion approach. *J. Chem. Phys.* **2013**, *138*, 045101.
(26) Peng, Q.; Yi, Y.; Shuai, Z.; Shao, J. Toward Quantitative Prediction of Molecular Fluorescence Quantum Efficiency: Role of Duschinsky Rotation. *J. Am. Chem. Soc.* **2007**, *129*, 9333−9339.
(27) Niu, Y.; Peng, Q.; Shuai, Z. Promoting-mode free formalism for excited state radiationless decay process with Duschinsky rotation effect. *Sci. China, Ser. B: Chem.* **2008**, *51*, 1153−1158.
(28) Mason, R. The crystallography of anthracene at 95°K and 290°K. *Acta Crystallogr.* **1964**, *17*, 547−555.
(29) Chen, P.-Z.; Weng, Y.-X.; Niu, L.-Y.; Chen, Y.-Z.; Wu, L.-Z.; Tung, C.-H.; Yang, Q.-Z. Light-Harvesting Systems Based on Organic Nanocrystals To Mimic Chlorosomes. *Angew. Chem., Int. Ed.* **2016**, *55*, 2759−2763.
(30) Winiger, C. B.; Li, S.; Kumar, G. R.; Langenegger, S. M.; Häner, R. Long-Distance Electronic Energy Transfer in Light-Harvesting Supramolecular Polymers. *Angew. Chem., Int. Ed.* **2014**, *53*, 13609−13613.
(31) Shuai, Z. G.; Peng, Q. Organic light-emitting diodes: theoretical understanding of highly efficient materials and development of computational methodology. *Natl. Sci. Rev.* **2017**, *4*, 224−239.
(32) Tal-Ezer, H.; Kosloff, R. An accurate and efficient scheme for propagating the time-dependent Schrödinger-equation. *J. Chem. Phys.* **1984**, *81*, 3967−3971.
(33) Leforestier, C.; Bisseling, R. H.; Cerjan, C.; Feit, M. D.; Friesner, R.; Guldberg, A.; Hammerich, A.; Jolicard, G.; Karrlein, W.; Meyer, H.-D.; Lipkin, N.; Roncero, O.; Kosloff, R. A comparison of different propagation schemes for the time dependent Schrödinger equation. *J. Comput. Phys.* **1991**, *94*, 59−80.
(34) Sherwood, P.; de Vries, A. H.; Guest, M. F.; Schreckenbach, G.; Catlow, C. R. A.; French, S. A.; Sokol, A. A.; Bromley, S. T.; Thiel, W.; Turner, A. J.; et al. QUASI: A general purpose implementation of the QM/MM approach and its application to problems in catalysis. *J. Mol. Struct.: THEOCHEM* **2003**, *632*, 1−28.
(35) Smith, W.; Forester, T. R. DL_POLY_2.0: A general-purpose parallel molecular dynamics simulation package. *J. Mol. Graphics* **1996**, *14*, 136−141.
(36) Wang, J.; Wolf, R. M.; Caldwell, J. W.; Kollman, P. A.; Case, D. A. Development and testing of a general amber force field. *J. Comput. Chem.* **2004**, *25*, 1157−1174.
(37) Bakowies, D.; Thiel, W. Hybrid Models for Combined Quantum Mechanical and Molecular Mechanical Approaches. *J. Phys. Chem.* **1996**, *100*, 10580−10594.
(38) Reimers, J. R. A practical method for the use of curvilinear coordinates in calculations of normal-mode-projected displacements and Duschinsky rotation matrices for large molecules. *J. Chem. Phys.* **2001**, *115*, 9103−9109.
(39) Niu, Y. L.; Li, W. Q.; Peng, Q.; Geng, H.; Yi, Y. P.; Wang, L. J.; Nan, G. J.; Wang, D.; Shuai, Z. G. MOlecular MAterials Property Prediction Package (MOMAP) 1.0: a software package for predicting the luminescent properties and mobility of organic functional materials. *Mol. Phys.* **2018**, *116*, 1078−1090.
(40) Hsu, C.-P. The Electronic Couplings in Electron Transfer and Excitation Energy Transfer. *Acc. Chem. Res.* **2009**, *42*, 509−518.
(41) Valiev, M.; Bylaska, E. J.; Govind, N.; Kowalski, K.; Straatsma, T. P.; Van Dam, H. J. J.; Wang, D.; Nieplocha, J.; Apra, E.; Windus, T. L.; de Jong, W. A. NWChem: A comprehensive and scalable open-source solution for large scale molecular simulations. *Comput. Phys. Commun.* **2010**, *181*, 1477−1489.
(42) Mulder, B. J. Diffusion and Surface Reactions of Singlet Excitons in Anthracene. *Philips Research Reports*; Philips Research Laboratories, 1968.
(43) Peng, Q.; Niu, Y.; Shi, Q.; Gao, X.; Shuai, Z. Correlation Function Formalism for Triplet Excited State Decay: Combined Spin−Orbit and Nonadiabatic Couplings. *J. Chem. Theory Comput.* **2013**, *9*, 1132−1143.
(44) Nijegorodov, N.; Ramachandran, V.; Winkoun, D. P. The dependence of the absorption and fluorescence parameters, the intersystem crossing and internal conversion rate constants on the number of rings in polyacene molecules. *Spectrochim. Acta, Part A* **1997**, *53*, 1813−1824.
(45) Shimura, H.; Ohba, Y. Time-resolved reabsorption effect on the fluorescence decay of anthracene crystal and solution. *Jpn. J. Appl. Phys.* **1981**, *20*, 1683−1690.
(46) Birks, J. B. The Influence of Reabsorption and Defects on Anthracene Crystal Fluorescence. *Mol. Cryst. Liq. Cryst.* **1974**, *28*, 117−129.
(47) Chen, P.-Z.; Zhang, H.; Niu, L.-Y.; Zhang, Y.; Chen, Y.-Z.; Fu, H.-B.; Yang, Q.-Z. A Solid-State Fluorescent Material Based on Carbazole-Containing Difluoroboron β-Diketonate: Multiple Chromisms, the Self-Assembly Behavior, and Optical Waveguides. *Adv. Funct. Mater.* **2017**, *27*, 1700332.

DOI: 10.1021/acs.jpcc.8b06918
J. Phys. Chem. C 2018, 122, 18365−18375

(48) Shao, Y.; Molnar, L. F.; Jung, Y.; Kussmann, J.; Ochsenfeld, C.; Brown, S. T.; Gilbert, A. T. B.; Slipchenko, L. V.; Levchenko, S. V.; O'Neill, D. P.; et al. Advances in methods and algorithms in a modern quantum chemistry program package. *Phys. Chem. Chem. Phys.* **2006**, *8*, 3172−3191.
(49) Li, W.; Peng, Q.; Xie, Y.; Zhang, T.; Shuai, Z. Effect of intermolecular excited-state interaction on vibrationally resolved optical spectra in organic molecular aggregates. *Acta Chim. Sin.* **2016**, *74*, 902−909.
(50) Donati, D.; Williams, J. O. Exciton Diffusion Lengths for Pure and Doped Anthracene Single Crystals from Microscopic Measurements. *Mol. Cryst. Liq. Cryst.* **1978**, *44*, 23−32.

DOI: 10.1021/acs.jpcc.8b06918
J. Phys. Chem. C 2018, 122, 18365−18375